In vivo imaging reveals that pregabalin inhibits cortical spreading depression and propagation to subcortical brain structures

Authors:

Stuart M Cain[1,2], Barry Bohnet[3], Jeffrey M LeDue[2], Andrew C Yung[3], Esperanza Garcia[1,2], John R Tyson[1,2], Sascha RA Alles[1,2], Huili Han[2], Arn MJM van den Maagdenberg[4], Piotr Kozlowski[3], Brian A MacVicar[2] & Terrance P Snutch[1,2*]

Affiliations:

[1]Michael Smith Laboratories, University of British Columbia, Vancouver, Canada

[2]Djavad Mowafagian Center for Brain Health, University of British Columbia, Vancouver, Canada

[3]7T-MRI Facility, University of British Columbia, Vancouver, Canada

[4]Departments of Human Genetics and Neurology, Leiden University Medical Center, Leiden, The Netherlands

***Corresponding author**:

Dr. Terrance P. Snutch, Michael Smith Laboratories, 219-2185 East Mall, University of British Columbia, Vancouver, BC, Canada, V6T 1Z4, Phone: 604-822-6968, Email: snutch@msl.ubc.ca

Abstract

Migraine is characterized by severe headaches that can be preceded by an aura likely caused by cortical spreading depression (SD). The anti-epileptic pregabalin (Lyrica) shows clinical promise for migraine therapy although its efficacy and mechanism of action are unclear. As detected by diffusion-weighted MRI (DW-MRI), in wild-type mice acute systemic administration of pregabalin increased the threshold to initiate SD *in vivo*. In familial hemiplegic migraine type 1 mutant mice expressing human mutations (R192Q and S218L) in the $Ca_V2.1$ (P/Q-type) calcium channel subunit, pregabalin slowed the propagation speed of SD *in vivo*. Acute systemic administration of pregabalin *in vivo* also selectively prevented the migration of SD into subcortical striatal and hippocampal regions in the R192Q strain that exhibit a milder phenotype and gain of $Ca_V2.1$ channel function. At the cellular level, pregabalin differentially inhibited glutamatergic synaptic transmission between wild-type, R192Q and S218L mice. Together, the study describes a novel DW-MRI analysis method for tracking the progression of SD and provides support and a mechanism of action for pregabalin as a possible effective therapy in the treatment of migraine.

Significance Statement

Spreading depression is a proposed to underlie migraine with aura, a type of debilitating headache. While few pharmacological treatments are available, the pain drug pregabalin has demonstrated initial, promising results for the treatment of migraine in the clinic. Utilizing animal models of congenital migraine and live brain imaging, Cain et al. describe the cortical and subcortical migration of the spreading depression wave. Further, pregabalin is shown to be effective at suppressing spreading depression initiation and wave speed and also to directly affect nerve cell signalling. Overall, the study

supports the therapeutic potential of pregabalin in both non-congenital migraineurs and patients with mild congenital migraine.

\body

Introduction

Migraine is a common debilitating episodic brain disorder that presents as severe headaches accompanied with other symptoms including nausea and vomiting. In approximately one-third of patients the headache phase is preceded by an aura, thought to be caused by cortical Spreading Depression (SD) (1). SD is characterized by electrocorticographic (ECG) silencing and a directly-coupled (DC) potential shift that is generated by a spreading neuronal and glial depolarization. In addition to the aura in migraine, SD is associated with various pathological conditions, such as epilepsy, ischaemic stroke and subarachnoid haemorrhage (2–4). The SD wave front of brief neuronal excitation is followed by a long-lasting depolarization and travels rostrally at a speed of 2-6 mm/min rendering invaded tissue inactive (5). SD induces cell swelling and the release of various neuroactive factors including glutamate, potassium, protons and prostaglandins that together contribute to the pathophysiological process (4). A clue to the importance of SD in migraine comes from the fact that in experimental models cortical SD triggers downstream headache mechanisms through activation of trigeminal nerves and brainstem nuclei (6).

Familial hemiplegic migraine (FHM) is a monogenic form of migraine with aura accompanied by hemiparesis (1). FHM type 1 (FHM-1) is caused by missense mutations in the *CACNA1A* gene that encodes the α_{1A} subunit of voltage-gated $Ca_V2.1$ (P/Q-type) calcium channels (7). FHM-1 mutations introduced into the orthologous *Cacna1a* gene produce transgenic mice with phenotypes that closely

mimic both the milder (R192Q) and more severe (S218L) symptoms described in FHM-1 patients with these mutations (8, 9). FHM-1 mutations have been shown to produce an overall "gain-of-function" increase in calcium conductance at physiological membrane potentials (10, 11) which, due to the well-established role of the channels in calcium-mediated vesicular neurotransmitter release can explain the increased synaptic activity observed in the mutant animals (12–16).

While a number of preventative and abortive treatments are available, not all migraines are effectively treated and hospitalization can be necessary for prolonged migraine attacks (2, 17). Gabapentinoids (gabapentin and pregabalin) are clinically utilized, small molecule drugs used in the treatment of neuropathic pain and partial seizures. Gabapentin was initially designed as a GABA analogue, whereas pregabalin was developed to modulate GABA metabolism, with the aim of generating new treatments for epilepsy. Instead, these drugs were shown to bind to the $\alpha_2\delta_{1/2}$ subunits of high-voltage-activated calcium channels with little direct effect on either GABA receptors or metabolism (18). Although, initial studies suggested that gabapentin may be effective in the treatment of migraine, it has since been shown to have only nominal potency in migraineurs (19). Pregabalin (Lyrica) displays more linear kinetics and longer half-life than gabapentin (20) and has shown initially encouraging results as a potential treatment for migraine (21–23), although additional evidence for clinical efficacy is required. While pregabalin's exact mechanism of action has not been deciphered it has been shown to acutely inhibit calcium currents (24) and chronically suppress calcium channel trafficking (25). Furthermore, pregabalin displays greater efficacy for P/Q-type ($Ca_V2.1$) channels over L-type ($Ca_V1.1$-$Ca_V1.4$) and N-type ($Ca_V2.2$) channels (26). While there exists some controversy over putative acute versus chronic molecular mechanisms, pregabalin has most convincingly been associated with a reduction in excitatory neurotransmitter release, further implicating $Ca_V2.1$ calcium channels (27).

Here, we examined FHM-1 mouse models to determine the effects of pregabalin on the threshold for SD initiation and the propagation speed of the SD wave front *in vivo* using a newly developed customized DW-MRI methodology. Employing this method of DW-MRI analysis we were able to track the spread of SD through the brain with proficient spatiotemporal accuracy. Furthermore, we correlated the findings on SD with *in vitro* analysis of pregabalin efficacy in acute brain slices using intrinsic optical signalling (IOS) and on spontaneous and evoked synaptic activity in the hippocampus.

Results

Pregabalin increases the threshold for SD in wild-type mice in vivo

To examine the full potential of our novel DW-MRI methodology in the intact brain and in response to pregabalin administration, anesthetized mice were scanned using DW-MRI to visualize the spread of SD *in vivo*. DW-MRI images were acquired as eight consecutive slices at 8-second time intervals for 13 minutes (see Methods). SD was initiated using dual carbon fiber electrodes implanted in the occipital cortex (**Figure 1a, Supplemental Figure S1**). Vehicle-treated WT and R192Q mice did not display a significant difference in SD threshold ([WT *vs* R192Q] P=0.21 ANOVA), whereas the threshold was significantly lower in vehicle-treated S218L mice ([WT *vs* S218L] P=0.02 ANOVA, [R192Q *vs* S218L], P=0.03 ANOVA; **Figure 1b**). Subsequently, scans were acquired in WT and FHM-1 mice following administration of pregabalin (160 mg/kg, i.p., 45-60 minutes prior to scanning). Pregabalin treatment significantly increased the SD threshold in WT mice, and while a trend towards increased threshold was observed in the R192Q and S218L groups a significant difference was not achieved for the FHM-1 strains ([WT control *vs* WT pregabalin] P=0.03 *t*-test, [R192Q control *vs* R192Q pregabalin] P=0.14 *t*-test, [S218L control *vs* S218L pregabalin] P = 0.15 *t*-test; **Figure 1b**).

The sequential DW-MRI slices and 8-second temporal resolution allowed tracking of the SD wave trajectory across the cortex. SD was first visible in slice 3 (bregma -5.00) corresponding to the electrode position in the occipital cortex (**Supplemental Figure S1**) and from this point, the wave front travelled both around the circumference of the cortex and anterior until reaching slice 8, the last slice acquired in the frontal cortex (**Supplemental videos 1-3**). Of note, the SD wave front did not invade the cerebellum (slices 1 and 2; **Supplemental Figure S1d**) in either WT (n=5) or FHM-1 (n=12) strains. SD could not be initiated in cerebellum even when stimulation electrodes were placed directly in the vermis of the cerebellar cortex suggesting that this region is refractory to SD (n=1).

Pregabalin slows SD speed in R192Q and S218L FHM-1 mutant mice in vivo

SD speed was calculated from the cortex as the wave front travelled from slice 5 to slice 8 (see Methods). Both R192Q and S218L mice displayed a faster SD than WT with the speed in S218L mice being faster than in R192Q mice ([WT *vs* R192Q] P=0.04 ANOVA, [WT *vs* S218L] P=0.001, [R192Q *vs* S218L], P=0.02 ANOVA; **Figure 1c, Supplemental videos 1-3**). Notably, pregabalin treatment significantly slowed SD speed in both R192Q and S218L strains, but had no effect in WT mice ([WT control vs WT pregabalin] P=0.23, [R192Q control *vs* R192Q pregabalin] P=0.003, [S218L control *vs* S218L pregabalin] P<0.0001 *t*-test; **Figure 1c, Supplemental videos 4-6**).

A previous report found that SD is constrained to the cortex in WT mice, but can invade the striatum in R192Q mice, and the striatum, hippocampus, and, occasionally thalamus in S218L mice (28). Our data generally are in line with these findings, except that we did not observe invasion of SD to thalamus in S218L animals (**Figure 2, Figure 3, Supplemental videos 1-3**). Of note, in R192Q mice we observed that SD invaded both the hippocampus and striatum albeit with a significant delay of up to 1 minute after the SD wave front had passed through the cortex. In contrast, in S218L mice the SD wave front moved almost simultaneously into cortical and subcortical structures, consistent with the larger gain-of-

function effect of this mutation. Notably, whereas pregabalin did not prevent the invasion to subcortical structures in S218L mice, it completely abolished spread into both striatum and hippocampus in 4 out of 5 R192Q mice tested (**Figure 2, Figure 3, Supplemental videos 2, 3, 5 and 6**).

To further enhance visualization and quantitative comparisons of DW-MRI images during SD, a custom Matlab script was designed to automatically detect the SD wave front and to represent it in each slice as a heatmap, wherein cold colours correspond to early and hot colours to late SD appearance, respectively. Representative examples shown in **Supplemental Figure S2** emphasise the cortical confinement of SD in WT mice and the subcortical invasion in FHM-1 mice. Furthermore, they confirm the marked delay in arrival of the SD wave front in striatum and hippocampus of R192Q mice. Finally, this image analysis tool confirmed that pregabalin administration slows SD speed in both strains of FHM-1 mice, and prevents subcortical invasion of SD in R192Q mice.

Pregabalin slows the speed of spreading depression in S218L mutant brain slices in vitro

To further examine pregabalin effects on SD, IOS imaging was utilized on acute brain slices from FHM-1 and WT mice. In this preparation SD is visualized as an increase in brightness resulting from increased transparency of the brain tissue caused by cell swelling during the depolarization (29). Bath application of 40 mM KCl induced SD in brain tissue, occasionally from more than one focal point (**Figure 4**). The SD wave front travelled across the cortex and invaded (and sometimes was initiated in) the caudate putamen in brain slices of both FHM-1 and WT mice (**Figure 4a**). In agreement with previous findings (8, 9) the speed of the cortical SD wave front was significantly faster in brain slices from R192Q and S218L animals compared with WT mice ([WT *vs* R192Q] P=0.01 ANOVA, [WT *vs* S218L] P=0.001 ANOVA; **Figure 4a and 4b**). Pregabalin pre-treatment (1 hour) had no significant effect on SD speed in brains slices from WT, while it significantly slowed SD speed in brain slices from both R192Q and

S218L animals (([WT control *vs* WT pregabalin] P=0.26 *t*-test, [R192Q control *vs* R192Q pregabalin] P=0.03 *t*-test, [S218L control *vs* S218L pregabalin] P=0.0005 *t*-test; **Figure 4b**). No significant difference in the degree of localized cell swelling, correlated with ΔIOS (29) was observed either between strains or as a result of pregabalin pre-treatment (**Figure 4c**).

Pregabalin acutely inhibits $Ca_V2.1$ calcium channel complexes containing the $\alpha_2\delta_1$ subunit

To confirm pregabalin effects on $Ca_V2.1$-mediated calcium currents, electrophysiological recordings were performed in human-derived neuroblastoma SH-SY5Y cells transiently expressing the recombinant human $Ca_V2.1$ subunit co-expressed with β_2 and either $\alpha_2\delta_1$ or $\alpha_2\delta_3$ auxiliary subunits. The effect of pregabalin pre-treatment was assessed at a concentration of 500 µM, previously reported to inhibit synaptic activity in the mouse brainstem auditory system (30). The peak calcium current amplitude elicited by repetitive square depolarizations from a holding potential of -110 mV to 0 mV was reduced by 27% (n=8) when 500 µM pregabalin was applied to SH-SY5Y cells expressing $Ca_V2.1$ co-transfected with the β_2 and $\alpha_2\delta_1$ subunits (**Figure 5a**). Conversely, currents obtained upon co-expression with the β_2 and $\alpha_2\delta_3$ subunits were unaffected by pregabalin (**Figure 5a**). The selective inhibitory effect on $Ca_V2.1$ channels co-expressed with $\alpha_2\delta_1$, but not $\alpha_2\delta_3$ ancillary subunits was observed across a range of voltage steps elicited by a current-voltage relationship (**Figure 5b**). These results are consistent with the high binding affinity of gabapentinoids to the $\alpha_2\delta_1$ subunit compared to $\alpha_2\delta_3$ (31).

Pregabalin suppresses spontaneous and evoked synaptic activity

We next examined whether effects of pregabalin on intrinsic neuronal excitability and/or synaptic activity levels could explain the differential alterations on the threshold and speed of SD in WT and FHM-1 mice. Whole-cell patch clamp recordings in hippocampal acute slices were used as the DW-MRI analyses revealed that SD invasion occurred in this region in S218L and R192Q, but not WT mice.

Potential differences in global hippocampal synaptic activity were investigated by recording spontaneous excitatory postsynaptic currents (sEPSCs; **Supplemental Figure S4b**) in the absence of any stimulation or current injection using whole-cell voltage-clamp with picrotoxin in the patch pipette to block GABAergic inhibitory PSCs (IPSCs). Pregabalin (500 μM) significantly reduced the amplitude and increased the sEPSC interval (i.e. decreased the frequency) in CA1 neurons in slices from both WT and R192Q mice (**Figure 5c-d, Supplemental Figure S3-S4a**). Rather unexpectedly, pregabalin was found to increase amplitude and decrease inter-event interval in S218L CA1 neurons. At a lower concentration (100 μM) pregabalin had no effect on sEPSC amplitude or frequency in WT, reduced the frequency of sEPSCs in both R192Q and S218L and increased the amplitude of sEPSCs in S218L CA1 neurons (**Figure 5e, Supplemental Figure S4b**).

To examine the effect of pregabalin on electrically evoked EPSPs (eEPSPs) in hippocampal slices, a paired-pulse stimulation protocol was applied to glutamatergic CA3 axons (Schaffer collaterals) while simultaneously recording voltage responses using current-clamp in CA1 soma (**Figure 5f**). To ameliorate cell-to-cell variability, eEPSP amplitude was normalized to the control eEPSP peak. While pregabalin (500 μM) significantly reduced the amplitude of eEPSPs in both WT and R192Q it had no significant effect on S218L CA1 neurons in response to Schaffer collateral stimulation. At a lower concertation pregabalin (100 μM) only inhibited eEPSP amplitude in R192Q CA1 neurons. No significant effect of pregabalin was observed on paired-pulse facilitation (**Figure 5f**).

Discussion

One aim of this study was to develop advanced neuroimaging methodologies that permit the *in vivo* visualization of SD in a three-dimensional, whole-brain perspective with a high temporal resolution. This has permitted further insight into the spatiotemporal dynamics of SD in both WT mice and those

displaying mild (R192Q) or severe (S218L) FHM-1 phenotypes (7). Further, we tested the hypothesis that pregabalin, an anti-epileptic with high-affinity binding to $\alpha_2\delta_1$–containing calcium channel complexes, may exhibit functional effects in FHM-1 and WT mice. Our key findings concerning SD and the actions of pregabalin are: 1) SD threshold and speed are differentially affected by R192Q and S218L FHM-1 mutations, 2) in both FHM-1 strains SD invades the striatum and hippocampus albeit with a notable delay in R192Q animals, 3) SD does not invade the cerebellum in any strain or under any stimulation protocol, 4) SD threshold is increased by pregabalin in WT but not FHM-1 mice, 5) pregabalin slows SD velocity in both FHM-1 strains but not WT mice, and 6) SD invasion of subcortical structures is suppressed by pregabalin in animals expressing the milder R192Q change but not the more severe S218L FHM-1 mutation.

SD threshold and speed are differentially affected by R192Q and S218L FHM-1 mutations

Compared to WT and R192Q animals we observed a lower SD threshold *in vivo* in S218L mice, suggesting that only the S218L $Ca_V2.1$ channel gain-of-function mutation was significantly pathophysiological to promote the initiation of SD as a result of cortical electrical depolarization. This finding was somewhat unexpected given previous data indicating a lowered SD threshold associated with both FHM-1 mutations (8, 9) and also in that both R192Q and S218L mice display enhanced glutamatergic activity in cortical neurons (15, 16, 32). Notably, in the current study isoflurane was used rather than urethane which may have differentially affected SD threshold. Also, the carbon fiber electrodes utilized for stimulation in the MRI scanner are larger in diameter than the metal electrodes utilized previously, which may have affected stimulation sensitivity (9). If stimulation threshold is modulated solely by the level of synaptic excitability, a lower SD threshold would be expected in both S218L and R192Q mice. Our findings may indicate that SD threshold is not linked directly to synaptic activity, but rather to enhanced basal neuronal excitability in the cortex. This notion fits with previous

data demonstrating that cortical neurons from S218L mice display calcium currents with a distinct leftward shift in activation properties that is less pronounced in R192Q mice (16). As a result, S218L neurons are predicted to have the ability to conduct calcium at rest, endowing them with the ability to modulate neuronal excitability at a range of membrane potentials normally considered subthreshold (13).

Although SD threshold was only found to be decreased in S218L animals, we observed an increase in cortical SD conduction velocity in both R192Q and S218L FHM-1 strains, similar to that described previously (8, 9). The gain-of-function alterations of $Ca_V2.1$ channels containing R192Q or S218L mutations likely underlie the observed increases in SD speed in these strains and is supported by studies demonstrating enhanced synaptic activity in cortical neurons from both R192Q (15, 32) and S218L mice (16).

SD spreads to subcortical structures in both FHM-1 strains but not WT mice

Several mechanisms have been proposed for the spread of SD such as interneuronal-mediated signalling or passive diffusion of neuroactive substances through extracellular fluid (5). In R192Q mice, a progressive spread of SD to subcortical structures was observed particularly in slice 5 (bregma -2.50mm). Typically, the SD propagated ventro-lateral from the dorsal-medial cortex until reaching the entorhinal cortex, followed by the delayed appearance of SD first in the ventral hippocampus, then the dorsal hippocampus. Similarly, this pattern of SD propagation was observed in slice 6 in R192Q mice with SD spreading into the striatum (**Supplemental video 3, Figures 3, 4**). These results suggest that between certain interconnected areas, for example the entorhinal cortex-subiculum and piriform cortex-striatum there normally exist failure-points where SD propagation is limited and that a diffusional and/or synaptic barrier must be bridged in order for SD to further spread. We speculate that neurons expressing

$Ca_V2.1$ channels containing either R192Q or S218L mutations enable the spread of SD across subcortical failure-points.

Hippocampal SD has been reported previously after direct stimulation of the CA1 region in Sprague-Dawley rats (33) indicating that SD can indeed be initiated in this brain region but likely does not receive sufficient input during cortical SD and/or possesses a barrier preventing propagation of cortically-initiated SD. Invasion of SD into the striatum has been observed in some rat models (34) and in our IOS slice preparation we regularly observed SD invasion and initiation in striatum of WT mice. As WT animals did not display subcortical SD *in vivo* it is likely that similar to that for the hippocampus, the striatum is capable of SD but cannot normally propagate the wave in response to adjacent cortical SD. It has been suggested that in FHM-1 mice SD may spread to striatum and hippocampus via the amygdala and subiculum, respectively, and that lower neuronal densities in these areas may be responsible for limiting SD spread in WT animals (28). Our data from R192Q animals supports this view with respect to the anatomical entry point of SD into these structures for this strain. In S218L mice, in which SD immediately spreads to subcortical structures from the adjacent cortex, the stronger gain-of-function effect of the mutation on $Ca_V2.1$ channels apparently generates a sufficiently strong SD wave to span the corpus callosum. Of further interest is that for neither of the FHM-1 mutations was SD observed to propagate into the thalamus, although this has been reported to occur in a percentage of S218L mice (28). It should be considered that in the study by Eikermann-Haerter et al. electrophysiological measurements of SD were made under pentobarbital anesthesia, whereas our experiments were performed under isoflurane anesthesia, thus there may exist distinct effects of anesthetics concerning invasion of SD into the thalamus (35). Despite this difference, both studies indicate that the white matter of the internal capsule appears to be a particularly difficult region for SD to traverse.

It is noteworthy that we did not observe SD in the cerebellum, even when stimulation electrodes were placed directly into the cerebellar cortex. In agreement, cerebellar SD has not previously been reported in the FHM-1 mouse strains, although it has been observed in rats (36). Strong cerebellar symptoms in FHM-1 patients, including those with the S218L mutation are well-described and altered synaptic activity has been reported in cerebellar synapses in S218L mice (12, 37). Our results suggest that the FHM-1-mediated cerebellar symptoms are not associated with functional changes that might occur as a result of any recurrent SD within the cerebellum.

SD threshold is increased by pregabalin in WT but not FHM-1 mice

Gabapentin has been shown to increase the threshold for SD *in vivo* (38) and we hypothesized that pregabalin might also alter SD. Furthermore, gabapentin and pregabalin are known to bind to the $\alpha_2\delta_{1/2}$ auxiliary subunit of $Ca_V2.1$ calcium channels and that gabapentinoid-mediated inhibition of calcium currents has been reported both acutely (24, 39) and via chronic effects on channel trafficking (25, 30, 40). In the current study pregabalin was effective in increasing the threshold for stimulation to induce SD in WT, but not R192Q or S218L mice. This suggests that pregabalin may be an effective treatment for preventing migraine with aura in migraineurs without FHM-1 mutations. In contrast, in FHM-1 patients the gain-of-function phenotypes conferred to $Ca_V2.1$ channels may be too severe for pregabalin to be therapeutically efficacious. We did, however observe a trend towards increased threshold following acute pregabalin treatment in FHM-1 mice and, therefore pregabalin should not necessarily be ruled out as a chronically administered preventative treatment for FHM-1 patients.

Pregabalin slows SD in FHM-1 strains but not WT mice

We demonstrated that pregabalin slowed SD in S218L and R192Q but not WT mice. As discussed, cortical synapses that express $Ca_V2.1$ channels containing R192Q and S218L mutations display

enhanced excitatory, but not inhibitory neurotransmission (16, 32) and also that a leftward shift in the activation curve of $Ca_V2.1$ channels containing the S218L mutation allows calcium conduction at resting membrane potentials (16). Together this would permit subthreshold modulation of excitability by $Ca_V2.1$ in S218L mice providing a potential mechanism underlying the more severe phenotype in this strain. Pregabalin has a direct inhibitory effect on calcium-mediated glutamate release in brain slices from neocortex (41) and entorhinal cortex (42). In addition, pregabalin displays two- to three-fold enhanced efficacy of depression of noradrenaline release upon sustained depolarization compared to brief stimulation (26, 43). The long-lasting depolarization during that occurs during SD may further increase the efficacy of pregabalin on neurotransmitter release when attenuating the synaptic gain-of-function resulting from R192Q and S218L mutations. Overall, that pregabalin is more effective at slowing SD speed in FHM-1 compared to WT mice directly supports our hypothesis that pregabalin has a functional inhibitory effect on native $Ca_V2.1$ channels.

SD invasion of subcortical structures is abolished by pregabalin in R192Q mice

A notable finding from our DW-MRI experiments is that pregabalin prevented the subcortical invasion of SD in 4 out of 5 R192Q animals. Given that pregabalin did not prevent subcortical invasion in S218L mice, we would argue that pregabalin sufficiently suppresses excitability to prevent SD propagation through failure-points in the milder R192Q phenotype mice to block spread into subcortical structures. Previous studies have demonstrated that pregabalin inhibits vesicle trafficking in hippocampal neurons, reducing the readily-releasable pool (44) and attenuating vesicle release (45). In hippocampal brain slices, we observed that pregabalin (500 μM) effectively suppressed both spontaneous and evoked synaptic activity in WT and R192Q CA1 neurons, but not in S218L CA1 neurons. This strain-specific inhibition of evoked synaptic function provides a molecular mechanism for pregabalin to suppress the invasion of the hippocampus in R192Q mice, but not S218L mice. While SD did not spontaneously

invade the hippocampus in WT mice, its efficacy on synaptic activity in WT CA1 neurons suggests that pregabalin may provide an effective preventative treatment to limit subcortical progression of migraine in non-FHM-1 migraineurs as well as for milder forms of FHM-1.

In summary, we find that SD is limited to defined brain regions by as yet unknown synaptic and/or diffusional barriers involving $Ca_V2.1$ (P/Q-type) calcium channel-mediated excitability and that these barriers can be bridged by the consequences of FHM-1 mutations. Furthermore, pregabalin is effective towards increasing the threshold for SD in WT animals, in slowing SD velocity in FHM-1 mice, as well as preventing SD subcortical propagation associated with the milder R192Q FHM-1 mutation. These findings support the notion that pregabalin may be effective acutely but have not addressed its effects on chronic drug administration. While gabapentin has recently fallen from favour as a preventative treatment in migraine (19), initial reports on the use of pregabalin are encouraging (21–23). The current study provides new insights into the mechanism of action of pregabalin and supports its therapeutic potential in both non-FHM migraineurs and patients with milder FHM-1 mutations.

Acknowledgements:

Supported by a Brain Canada Multi-Investigator Research Initiative Grant with matching support from Genome BC, MSFHR, and the Koerner Foundation. T.P. Snutch and S.M. Cain were supported by a Pfizer Neuropathic Pain Award. T.P. Snutch is supported by an operating grant from CIHR (#10677) and the CRC in Biotechnology and Genomics-Neurobiology. S.M. Cain was supported by a research grant from the BC Epilepsy Society. B.A.M. supported by the CRC in Neuroscience, CIHR operating grants (#148397, #8545, #115121 and TCE-117869 ERA-NET NEURON) and Fondation Leducq.

Materials and Methods

Animals

Wild-type (WT), as well as transgenic R192Q (8)and S218L littermate (9) postnatal day (P)20-P40 male and female mice were used in all experiments in accordance with CCAC guidelines and genotyped as previously described (9).

Heterologous expression and electrophysiology of recombinant $Ca_V2.1$ calcium channels

The human neuroblastoma cell line SH-SY5Y (ATTC CRL-2266) was cultured in a 1:1 mixture of Eagle's Minimal Essential Media (Sigma, USA) and F-12 Media (Invitrogen, USA), supplemented with 0.5 mM sodium pyruvate and 10% fetal bovine serum. Cells were seeded on poly-D-Lysine (0.1 mg/mL) coated glass coverslips 24 h before transfection. Recombinant human $Ca_V2.1$ α_1 subunit was co-transfected with β_4 and $\alpha_2\delta_1$ or $\alpha_2\delta_3$ auxiliary subunits at a 1:1:1 molar ratio, and with a plasmid encoding the reporter GFP (1:10 ratio). GeneXPlus (ATTC, ACS-4004) transfection agent was used according to the procedure provided by the supplier. Whole-cell patch-clamp recordings were performed at room temperature 48 h after transfection.

Acute brain slice preparation

Animals were anesthetized using isoflurane (5% in air), sacrificed by cervical dislocation, the brains rapidly removed and transferred to ice cold sucrose-artificial cerebral spinal fluid (sucrose-aCSF) containing (mM): 214 sucrose, 26 $NaHCO_3$, 1.25 NaH_2PO_4, 11 glucose, 2.5 KCl , 0.5 $CaCl_2$, 6 $MgCl_2$, bubbled with 95% O_2:5% CO_2. Brain tissue was glued to a cutting chamber in a vibrating microtome (VT 1200, Leica, USA), which was then filled with ice cold sucrose-aCSF.

Intrinsic optical signalling

Coronal brain slices (350 μm thick) were cut at the level of the striatum and incubated at 33-35ºC in aCSF containing (mM): 126 NaCl, 2.5 KCl, 26 $NaHCO_3$, 1.5 NaH_2PO4, 2 $CaCl_2$, 2 $MgCl_2$, 10 glucose; bubbled with 95% O_2:5% CO_2. Slices were transferred to a recording chamber superfused with aCSF and maintained at 33-35ºC. Slices were pretreated with pregabalin or aCSF (control) for 60 minutes and continued via the perfusate for the duration of the experiment (29) (see Supplemental Materials and Methods).

Acute brain slice patch clamp electrophysiology

Horizontal brain slices (350 μm thick) were cut from the level of the ventral hippocampus and incubated at 33-35ºC in aCSF bubbled with 95% O_2:5% CO_2. Slices were transferred to a recording chamber superfused with aCSF and maintained at 33-35ºC (see Supplementary Materials and Methods).

Magnetic resonance imaging

Animals were anesthetized using isoflurane for the duration of surgical preparation and MRI scanning. Mice were placed in a stereotaxic frame and an incision made in the scalp. Two holes were drilled in the skull over the right hemisphere of the visual cortex (hole 1 = bregma -4.5 mm, lateral 1.5 mm; hole 2 = bregma -4.5mm, lateral 2.5 mm) and sterile carbon fiber electrodes (WPI, USA) inserted into each hole to a depth of 0.5mm into the cortex. Glue was used to cement the electrodes into position and the wound sutured and covered with surgical tape. The mouse was laid supine in the MRI cradle and the stimulation electrodes fed through the centre of a custom RF coil, and then connected to a constant current unit exterior to the magnet bore and controlled via a simulator (Grass Technologies, USA). Respiratory and heart rate was monitored during scanning to control anesthesia depth.

MRI experiments were carried out on a 7 Tesla animal scanner (Bruker, Germany). Some 70 mm i.d. volume RF coil was used for pulse transmission and the MRI signal was received with a 14 mm diameter actively decoupled surface coil. T2-weighted MRI was used to acquire high-resolution structural images prior to DW-MRI scanning. DW-MRI was acquired using diffusion-weighted spin-echo EPI with a b-value of 1800 s/mm^2 (echo time/repetition time = 29/2000 ms, 4 shots, field of view = 2x2 cm, matrix size = 64x64, slice thickness = 1.25 mm, 8 interleaved slices, 100 repetitions in 13 min 20 sec) in 13 minute intervals, during which four stimulations would be applied to the visual cortex at 1, 4, 7 and 10 minutes. Stimulation intensity was started at 0.25 mA x 100ms (25 µC) and the amperage or duration increased to generate an incrementally increasing charge stimulation [scan set 1 (25, 50, 100, 200), scan set 2 (300, 400, 500, 600), scan set 3 (700, 800, 900, 1000) µC]. The 13-minute DW-MRI scan was repeated with the next level of stimulation intensities if no SD occurred.

Drugs

Pregabalin (generously provided by Pfizer) was dissolved directly in extracellular solution for heterologous expression system experiments, aCSF for *in vitro* acute brain slice and in 0.9% sterile saline (10 mL/kg) for *in vivo* MRI experiments.

Data analysis

Electrophysiological data analysis was performed using Clampfit (v9 and v10, Molecular Devices). IOS was performed using Zen (Blue edition, Zeiss) and ImageJ (v 1.50d, NIH). DW-MRI analyses were performed using MATLAB (v 2014a, Mathworks) and ImageJ (v 1.50d, NIH). 3D reconstruction was performed using VisIt (v2.9.1, Lawrence Livermore National Laboratory). Graphing and statistical analyses were performed using Origin (v8.6, OriginLab). Data followed a normal distribution and statistical significance was calculated using Student's two-sample *t*-test (paired where relevant). One-

Way ANOVA with Tukey's post-hoc test was used for multiple comparisons. Cumulative distributions were compared using the Kologorov-Smirnov test. Data are plotted as mean ± standard error.

References:

1. Headache Classification Committee of the International Headache Society (IHS) (2013) The International Classification of Headache Disorders, 3rd edition (beta version). *Cephalalgia* 33(9):629–808.
2. Dreier JP (2011) The role of spreading depression, spreading depolarization and spreading ischemia in neurological disease. *Nat Med* 17(4):439–447.
3. Hadjikhani N, et al. (2001) Mechanisms of migraine aura revealed by functional MRI in human visual cortex. *Proc Natl Acad Sci USA* 98(8):4687–4692.
4. Lauritzen M, et al. (2011) Clinical relevance of cortical spreading depression in neurological disorders: migraine, malignant stroke, subarachnoid and intracranial hemorrhage, and traumatic brain injury. *J Cereb Blood Flow Metab* 31(1):17–35.
5. Pietrobon D, Moskowitz MA (2014) Chaos and commotion in the wake of cortical spreading depression and spreading depolarizations. *Nat Rev Neurosci* 15(6):379–393.
6. Karatas H, et al. (2013) Spreading depression triggers headache by activating neuronal Panx1 channels. *Science* 339(6123):1092–1095.
7. Ferrari MD, Klever RR, Terwindt GM, Ayata C, van den Maagdenberg AMJM (2015) Migraine pathophysiology: lessons from mouse models and human genetics. *Lancet Neurol* 14(1):65–80.
8. van den Maagdenberg AM, et al. (2004) A Cacna1a knockin migraine mouse model with increased susceptibility to cortical spreading depression. *Neuron* 41(5):701–10.
9. van den Maagdenberg AM, et al. (2010) High cortical spreading depression susceptibility and migraine-associated symptoms in Ca(v)2.1 S218L mice. *Ann Neurol* 67(1):85–98.
10. Adams PJ, et al. (2009) Ca(V)2.1 P/Q-type calcium channel alternative splicing affects the functional impact of familial hemiplegic migraine mutations: implications for calcium channelopathies. *Channels* 3(2):110–21.
11. Tottene A, et al. (2005) Specific kinetic alterations of human CaV2.1 calcium channels produced by mutation S218L causing familial hemiplegic migraine and delayed cerebral edema and coma after minor head trauma. *J Biol Chem* 280(18):17678–17686.
12. Adams PJ, et al. (2010) Contribution of calcium-dependent facilitation to synaptic plasticity revealed by migraine mutations in the P/Q-type calcium channel. *Proc Natl Acad Sci U S A* 107(43):18694–9.
13. Di Guilmi MN, et al. (2014) Synaptic gain-of-function effects of mutant Cav2.1 channels in a mouse model of familial hemiplegic migraine are due to increased basal [Ca2+]i. *J Neurosci* 34(21):7047–7058.
14. Kaja S, et al. (2010) Severe and progressive neurotransmitter release aberrations in familial hemiplegic migraine type 1 Cacna1a S218L knock-in mice. *J Neurophysiol* 104(3):1445–1455.
15. Tottene A, et al. (2009) Enhanced excitatory transmission at cortical synapses as the basis for facilitated spreading depression in Ca(v)2.1 knockin migraine mice. *Neuron* 61(5):762–773.

16. Vecchia D, Tottene A, van den Maagdenberg AMJM, Pietrobon D (2015) Abnormal cortical synaptic transmission in CaV2.1 knockin mice with the S218L missense mutation which causes a severe familial hemiplegic migraine syndrome in humans. *Front Cell Neurosci* 9:8.

17. Gelfand AA, Goadsby PJ (2012) A Neurologist's Guide to Acute Migraine Therapy in the Emergency Room. *Neurohospitalist* 2(2):51–59.

18. Li Z, et al. (2011) Pregabalin is a potent and selective ligand for α(2)δ-1 and α(2)δ-2 calcium channel subunits. *Eur J Pharmacol* 667(1–3):80–90.

19. Linde M, Mulleners WM, Chronicle EP, McCrory DC (2013) Gabapentin or pregabalin for the prophylaxis of episodic migraine in adults. *Cochrane Database Syst Rev* 6:CD010609.

20. Bockbrader HN, et al. (2010) A comparison of the pharmacokinetics and pharmacodynamics of pregabalin and gabapentin. *Clin Pharmacokinet* 49(10):661–669.

21. Bakhshandeh Bali M, et al. (2015) Comparison of propranolol and pregabalin for prophylaxis of childhood migraine: a randomised controlled trial. *Acta Med Iran* 53(5):276–280.

22. Calandre EP, Garcia-Leiva JM, Rico-Villademoros F, Vilchez JS, Rodriguez-Lopez CM (2010) Pregabalin in the treatment of chronic migraine: an open-label study. *Clin Neuropharmacol* 33(1):35–39.

23. Pizzolato R, Villani V, Prosperini L, Ciuffoli A, Sette G (2011) Efficacy and tolerability of pregabalin as preventive treatment for migraine: a 3-month follow-up study. *J Headache Pain* 12(5):521–525.

24. Uchitel OD, Di Guilmi MN, Urbano FJ, Gonzalez-Inchauspe C (2010) Acute modulation of calcium currents and synaptic transmission by gabapentinoids. *Channels (Austin)* 4(6):490–496.

25. Bauer CS, et al. (2010) The anti-allodynic alpha(2)delta ligand pregabalin inhibits the trafficking of the calcium channel alpha(2)delta-1 subunit to presynaptic terminals in vivo. *Biochem Soc Trans* 38(2):525–528.

26. Dooley DJ, Donovan CM, Meder WP, Whetzel SZ (2002) Preferential action of gabapentin and pregabalin at P/Q-type voltage-sensitive calcium channels: inhibition of K+-evoked [3H]-norepinephrine release from rat neocortical slices. *Synapse* 45(3):171–190.

27. Dworkin RH, Kirkpatrick P (2005) Pregabalin. *Nat Rev Drug Discov* 4(6):455–456.

28. Eikermann-Haerter K, et al. (2011) Enhanced subcortical spreading depression in familial hemiplegic migraine type 1 mutant mice. *J Neurosci* 31(15):5755–5763.

29. Zhou N, Gordon GRJ, Feighan D, MacVicar BA (2010) Transient swelling, acidification, and mitochondrial depolarization occurs in neurons but not astrocytes during spreading depression. *Cereb Cortex* 20(11):2614–2624.

30. Di Guilmi MN, Urbano FJ, Inchauspe CG, Uchitel OD (2011) Pregabalin modulation of neurotransmitter release is mediated by change in intrinsic activation/inactivation properties of ca(v)2.1 calcium channels. *J Pharmacol Exp Ther* 336(3):973–982.

31. Marais E, Klugbauer N, Hofmann F (2001) Calcium channel alpha(2)delta subunits-structure and Gabapentin binding. *Mol Pharmacol* 59(5):1243–1248.

32. Vecchia D, Tottene A, van den Maagdenberg AMJM, Pietrobon D (2014) Mechanism underlying unaltered cortical inhibitory synaptic transmission in contrast with enhanced excitatory transmission in CaV2.1 knockin migraine mice. *Neurobiol Dis* 69:225–234.

33. Herreras O, Largo C, Ibarz JM, Somjen GG, Rio RM del (1994) Role of neuronal synchronizing mechanisms in the propagation of spreading depression in the in vivo hippocampus. *J Neurosci* 14(11):7087–7098.

34. Vinogradova LV, Koroleva VI, Bures J (1991) Re-entry waves of Leao's spreading depression between neocortex and caudate nucleus. *Brain Res* 538(1):161–164.

35. Takagaki M, et al. (2014) Isoflurane suppresses cortical spreading depolarizations compared to propofol--implications for sedation of neurocritical care patients. *Exp Neurol* 252:12–17.

36. Fifkova E, Bures J, Koshtoyants OK, Krivanek J, Weiss T (1961) Leao's spreading depression in the cerebellum of rat. *Experientia* 17:572–573.

37. Gao Z, et al. (2012) Cerebellar Ataxia by Enhanced CaV2.1 Currents Is Alleviated by Ca2+-Dependent K+-Channel Activators in Cacna1aS218L Mutant Mice. *J Neurosci* 32(44):15533–15546.

38. Hoffmann U, Dileköz E, Kudo C, Ayata C (2010) Gabapentin suppresses cortical spreading depression susceptibility. *J Cereb Blood Flow Metab* 30(9):1588–1592.

39. Weissmann C, Di Guilmi MN, Urbano FJ, Uchitel OD (2013) Acute effects of pregabalin on the function and cellular distribution of CaV2.1 in HEK293t cells. *Brain Research Bulletin* 90:107–113.

40. Dolphin AC (2012) Calcium channel auxiliary α2δ and β subunits: trafficking and one step beyond. *Nature Reviews Neuroscience* 13(8):542–555.

41. Fink K, et al. (2002) Inhibition of neuronal Ca(2+) influx by gabapentin and pregabalin in the human neocortex. *Neuropharmacology* 42(2):229–236.

42. Cunningham MO, Woodhall GL, Thompson SE, Dooley DJ, Jones RSG (2004) Dual effects of gabapentin and pregabalin on glutamate release at rat entorhinal synapses in vitro. *Eur J Neurosci* 20(6):1566–1576.

43. Dooley DJ, Donovan CM, Pugsley TA (2000) Stimulus-dependent modulation of [(3)H]norepinephrine release from rat neocortical slices by gabapentin and pregabalin. *J Pharmacol Exp Ther* 295(3):1086–1093.

44. Holz RW (2006) Pharmacology meets vesicular trafficking at a central nervous system synapse: pregabalin effects on synaptic vesicle cycling in hippocampal neurons. *Mol Pharmacol* 70(2):444–446.

45. Micheva KD, Taylor CP, Smith SJ (2006) Pregabalin reduces the release of synaptic vesicles from cultured hippocampal neurons. *Mol Pharmacol* 70(2):467–476.

46. de Crespigny A, Röther J, van Bruggen N, Beaulieu C, Moseley ME (1998) Magnetic resonance imaging assessment of cerebral hemodynamics during spreading depression in rats. *J Cereb Blood Flow Metab Off J Int Soc Cereb Blood Flow Metab* 18(9):1008–1017.

47. Vartanian MG, et al. (2006) Activity profile of pregabalin in rodent models of epilepsy and ataxia. *Epilepsy Res* 68(3):189–205.

Figure Legends:

Figure 1: Diffusion-weighted magnetic resonance imaging (DW-MRI) *in vivo*. (a) Diagram showing setup for DW-MRI scanning. **(b)** Mean *in vivo* data for SD stimulation threshold in vehicle and pregabalin-pretreated mice (WT control = 35.0 ± 6.5 (n=5), R192Q control = 35.8 ± 9.3 µC (n=6), S218L control = 10.0 ± 2.2 µC (n=6); WT pregabalin = 96.0 ± 18.6 (n=5), R192Q pregabalin = 58.0 ±

10.2 (n=5), S218L pregabalin = 30.6 ± 11.4 μC (n=8)). **(e)** Mean data for wave front speed (WT control = 4.9 ± 0.2 (n=5), R192Q control = 6.4 ± 0.1 (n=6), S218L control = 7.7 ± 0.4 mm/min (n=6); WT pregabalin = 4.4 ± 0.3 (n=5), R192Q pregabalin = 5.3 ± 0.3 (n=5), S218L pregabalin = 6.3 ± 0.1 mm/min (n=8)). *P<0.05 One-way ANOVA with Tukey's post-hoc test (between strains) and paired sample *t*-test (control versus pregabalin treatment).

Figure 2: Cortical-striatal SD spread in WT and FHM-1 mice. (a). Representative coronal DW-MRI images at level of striatum (bregma -1.25mm) superimposed with images of pixel intensity during SD. **(b)** Coronal map corresponding to DW-MRI images in (**b**) (cortex (Cx), striatum (St)). **(c)** Time course plots of SD spread showing mean pixel intensity in ROIs defined in **(a)** and coronal map **(b)**. Scale bars = 50 s, 10 intensity units.

Figure 3: Cortical-hippocampal SD spread in WT and FHM-1 mice. (a) Representative coronal DW-MRI images at level of hippocampus (bregma -2.5mm) superimposed with images of pixel intensity during SD. **(b)** Coronal schematic corresponding to DW-MRI images in (**a-c**) (cortex (Cx), hippocampus (Hp), thalamus (Th)). **(c)** Time course of SD spread showing mean pixel intensity in ROIs in **(a, b).** Scale bars = 50 s, 10 a.b.u.

Figure 4: Intrinsic Optical Signal (IOS) imaging in acute coronal brain slices. (a) Representative brain slice images from WT, R192Q and S218L mice following KCl (40 mM) application to initiate SD. **(b)** Mean IOS data for SD wave front speed (WT control = 2.9 ± 0.3 (n=20), R192Q control = 5.4 ± 0.4 (n=16), S218L control = 5.8 ± 0.7 (n=14) mm/min; WT pregabalin = 2.5 ± 0.1 (n=14), R192Q pregabalin = 4.2 ± 0.3 (n=14), S218L pregabalin = 2.9 ± 0.9 mm/min (n=13)). **(c)** Mean data for ΔIOS signal in control and pregabalin-pretreated brain slices. *P<0.05 One-way ANOVA with Tukey's post-hoc test (between strains) and two-sample *t*-test (control versus pregabalin treatment).

Figure 5: Pregabalin acutely inhibits voltage activated $Ca_V2.1$ Ca^{2+} currents in SH-SY5Y neuroblastoma cells excitability and both spontaneous and evoked synaptic activity in acute hippocampal brain slices. (a) Time course of pregabalin (500 µM) on currents recorded from SH-SY5Y cells co-transfected with $Ca_v2.1$ α_1, β_4 and $\alpha_2\delta_1$ (n=8; left panel) or $\alpha_2\delta_3$ (n=4; right panel) subunits (*insets: representative currents*). Mean fractional inhibition is shown as an inset in right panel. **(b)** Mean $Ca_v2.1$ current density-voltage relationships obtained before and after the application of pregabalin. Insets show representative currents. **(c)** Schematic of slice preparation used in **(c-e)** utilizing whole-cell voltage-clamp in CA1 neurons. Mean data for effect of 500 µM pregabalin on sEPSC amplitude (top panel) and inter-event interval (bottom panel) (WT (n=7 cells; 4 animals), R192Q (n=6 cells; 4 animals), S218L (n=9 cells; 4 animals)). Scale bars = 100 ms, 10 pA. **(d)** Representative current traces taken from 60-second voltage-clamp recordings at CA1 soma showing effect of pregabalin (500 µM) on sEPSCs in WT, R192Q and S218L FHM-1 strains. **(e)** Mean data for effect of 100 µM pregabalin on sEPSC amplitude (top panel) and inter-event interval (bottom panel) (WT (n=5 cells; 3 animals), R192Q (n=4 cells; 3 animals), S218L (n=5 cells, 3 animals)) **(f)** Schematic of slice preparation used in **(f)** utilizing whole-cell current clamp in CA1 neurons with paired (1ms pulse, 67 ms interval) stimulation applied to CA3 axons. Top panel shows mean data for eEPSP amplitude in response to 500 µM pregabalin (WT (n=6 cells; 4 animals), R192Q (n=6 cells; 4 animals), S218L (n=8 cells; 4 animals)). Bottom panel shows mean data for eEPSP amplitude in response to 100 µM pregabalin (WT (n=5 cells; 3 animals), R192Q (n=4 cells; 3 animals), S218L (n=5 cells; 3 animals)). Insets show representative voltage traces for effect of pregabalin on eEPSPs in WT, R192Q and S218L hippocampal CA1 neurons (WT: n=6 cells; 4 animals, R192Q: n=6 cells; 4 animals, S218L: n=8 cells; 4 animals). Inset scale bars = 50 ms, 5 mV. *P<0.05.

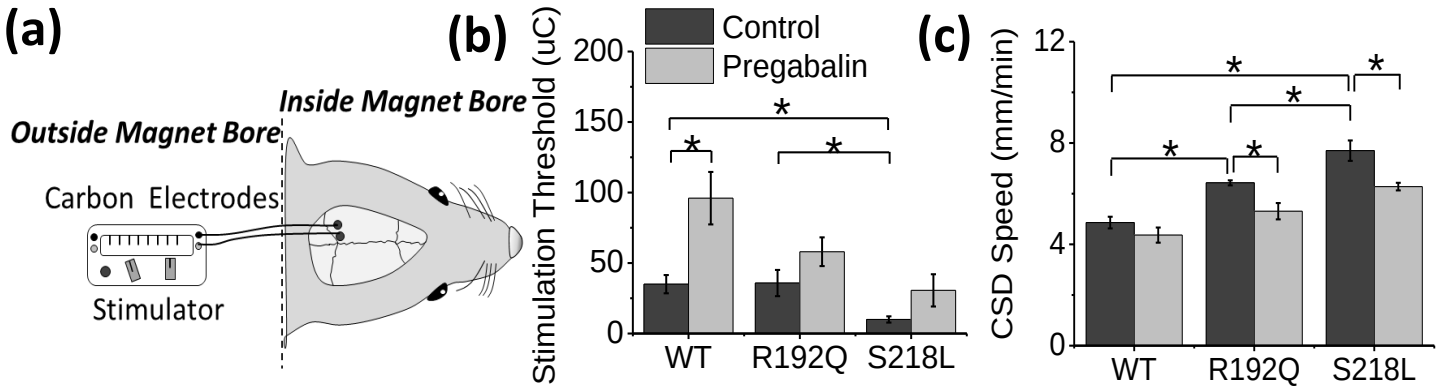
(a)
Inside Magnet Bore
Outside Magnet Bore
Carbon Electrodes
Stimulator
(b)
Control
Pregabalin
Stimulation Threshold (uC)
200
150
100
50
0
WT
R192Q
S218L
(c)
CSD Speed (mm/min)
12
8
4
0
WT
R192Q
S218L

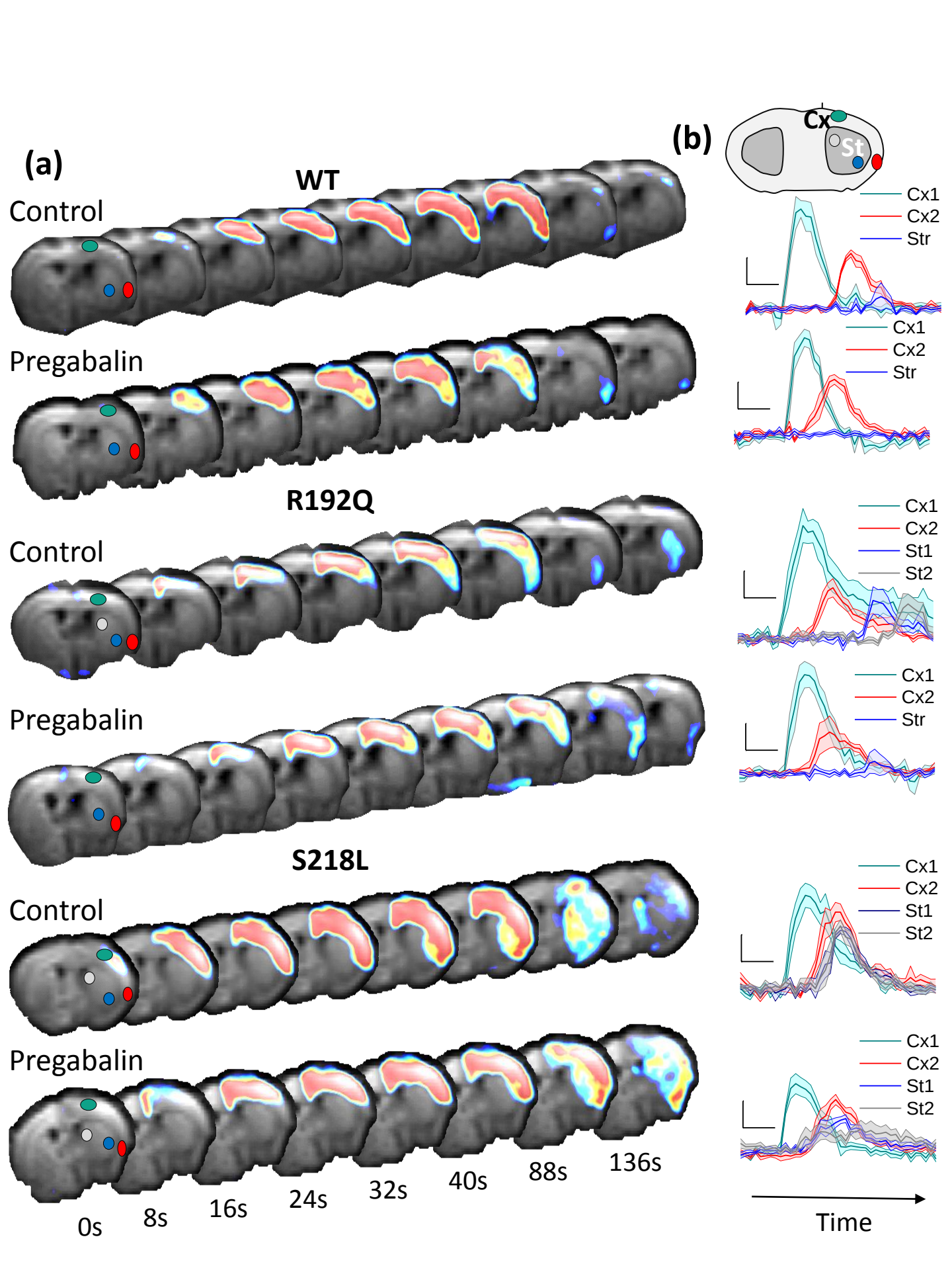
(a)
WT
Control
Pregabalin
R192Q
Control
Pregabalin
S218L
Control
Pregabalin
0s
8s
16s
24s
32s
40s
88s
136s
(b)
Cx
St
Cx1
Cx2
Str
St1
St2
Time

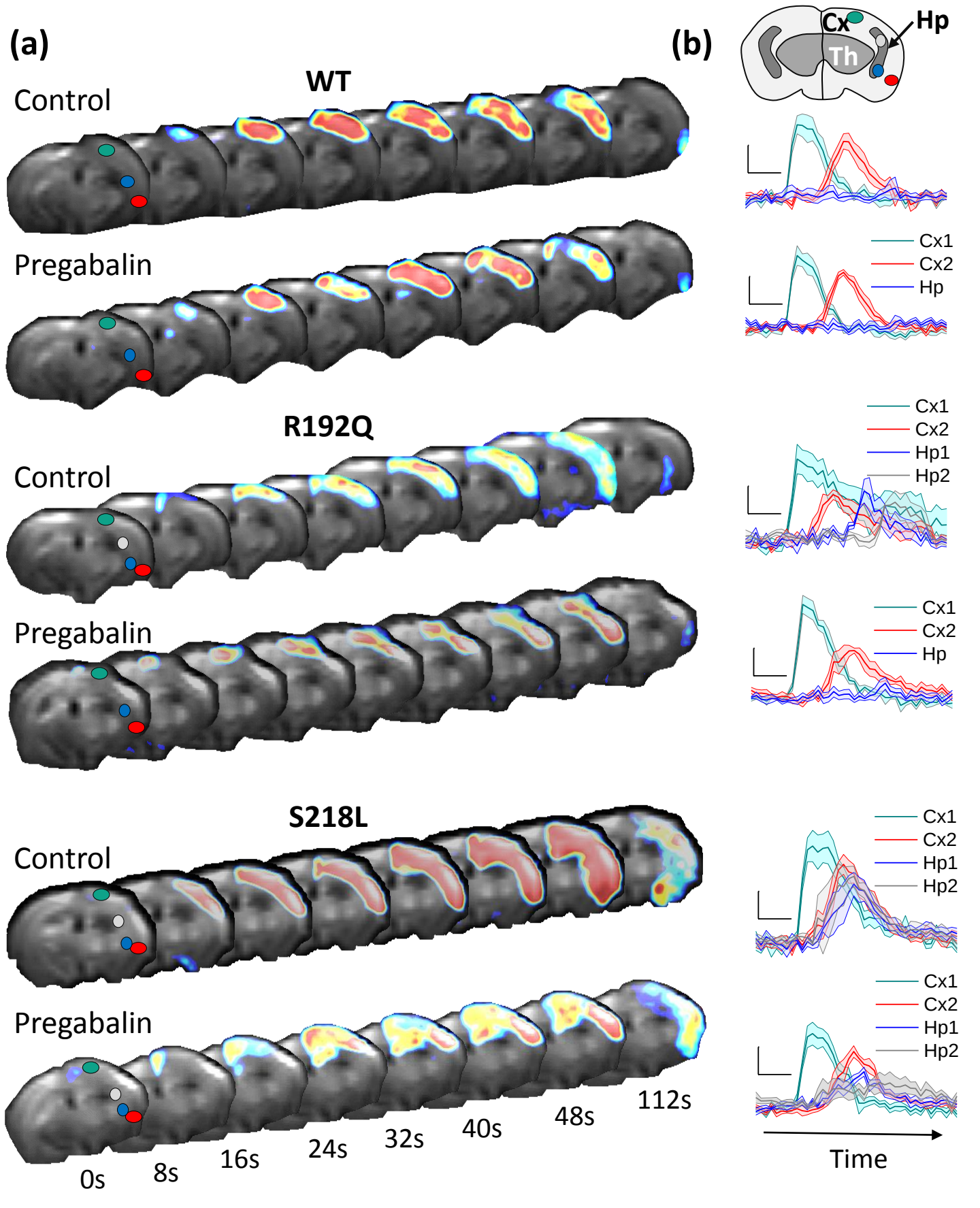
(a)
(b)
Cx
Hp
Th
WT
Control
Pregabalin
Cx1
Cx2
Hp
R192Q
Control
Pregabalin
Cx1
Cx2
Hp1
Hp2
S218L
Control
Pregabalin
0s
8s
16s
24s
32s
40s
48s
112s
Time

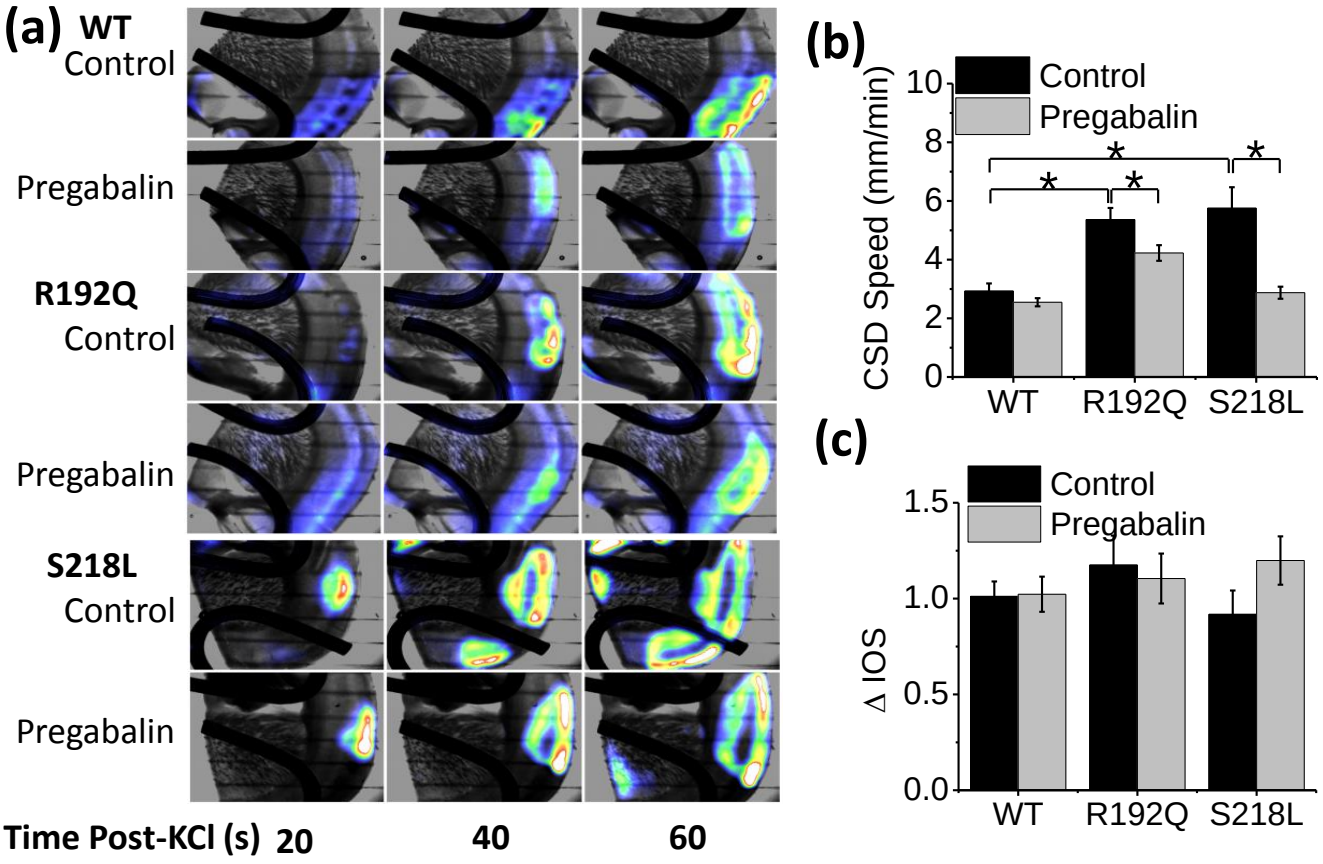
(a)
WT
Control
Pregabalin
R192Q
Control
Pregabalin
S218L
Control
Pregabalin
Time Post-KCl (s) 20 40 60
(b)
Control
Pregabalin
CSD Speed (mm/min)
0
2
4
6
8
10
WT
R192Q
S218L
(c)
Control
Pregabalin
Δ IOS
0.0
0.5
1.0
1.5
WT
R192Q
S218L

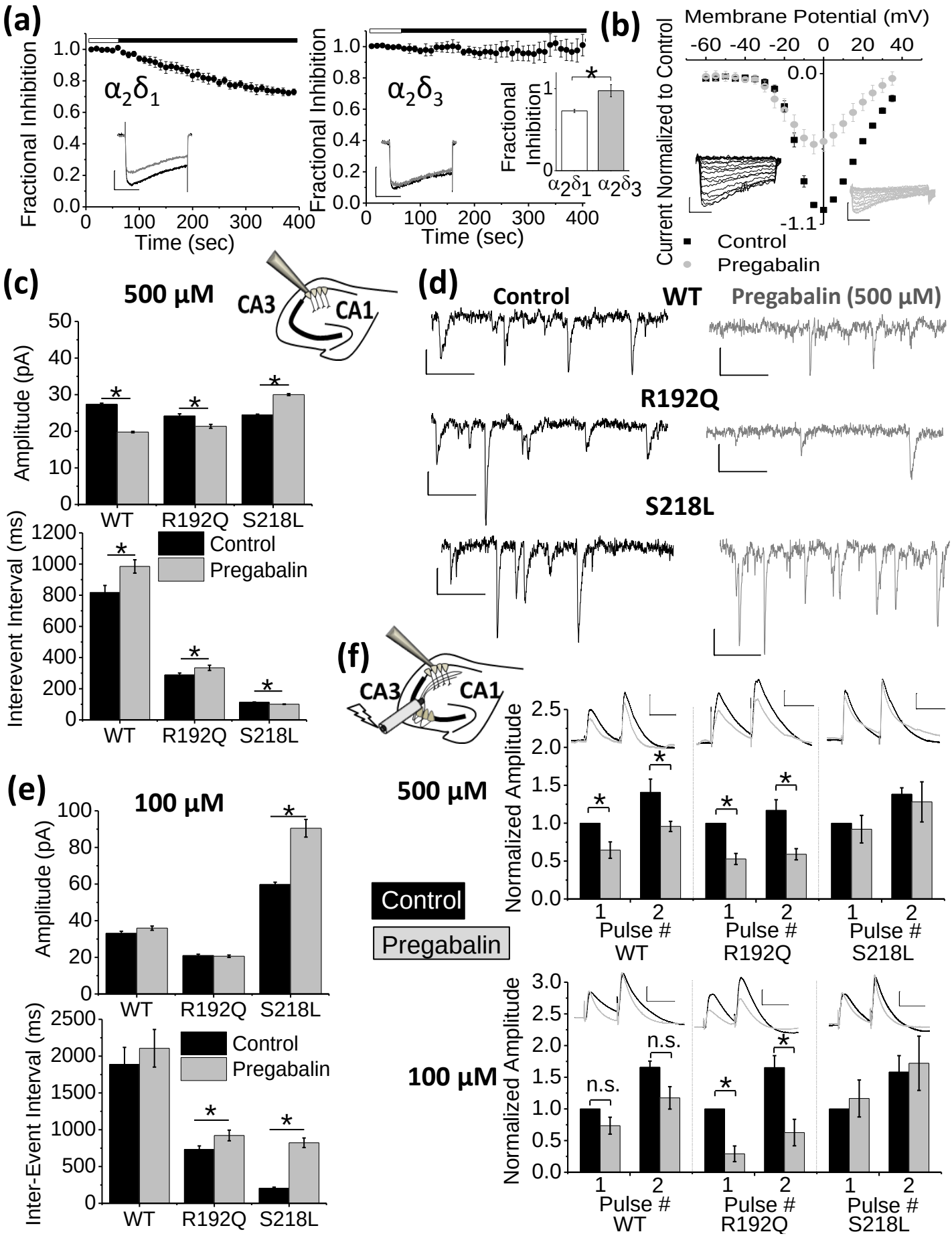
(a)
Fractional Inhibition
$\alpha_2\delta_1$
Time (sec)
$\alpha_2\delta_3$
Fractional Inhibition
$\alpha_2\delta_1$ $\alpha_2\delta_3$
(b)
Membrane Potential (mV)
Current Normalized to Control
Control
Pregabalin
(c)
500 µM
CA3
CA1
Amplitude (pA)
WT R192Q S218L
Interevent Interval (ms)
Control
Pregabalin
(d)
Control
WT
Pregabalin (500 µM)
R192Q
S218L
(e)
100 µM
Amplitude (pA)
Inter-Event Interval (ms)
(f)
CA3
CA1
500 µM
100 µM
Normalized Amplitude
Pulse #
n.s.